RSC Advances

ROYAL SOCIETY OF CHEMISTRY

www.rsc.org/advances

Structures and Alignment of Anisotropic Liquid Crystal Particles in a Liquid Crystal Cell

Jong-Hyun Lee[1], Tahseen Kamal[1], Stephan V. Roth[2], Peng Zhang[2], and Soo-Young Park[1*]

[1]Department of Polymer Science & Engineering, Kyungpook National University, #1370 Sangyuk-dong, Buk-gu, Daegu 702-701, Korea.

[2]HASYLAB at DESY, Notkestraße 85, D-22603 Hamburg, Germany.

*Corresponding author e-mail: psy@knu.ac.kr

Abstract: Anisotropic porous liquid crystal (LC) particles with ~ 60 μm diameters were prepared using microfluidics and directional UV photopolymerization of 1,4-bis-[4-(6-acryloyloxyhexyloxy)benzoyloxy]-2-methylbenzene/4-cyano-4'-pentylbiphenyl (RM257/5CB) mixtures at room temperature in the presence of a magnetic field. RM257 and 5CB in the RM257/5CB mixtures were reactive mesogen and orientation-inducible LC porogen, respectively. The RM257/5CB droplets coated with sodium dodecyl sulfate (SDS) ($RM257/5CB_{SDS}$) and poly(vinyl alcohol) (PVA) ($RM257/5CB_{PVA}$) showed radial and bipolar configurations, respectively, while UV photopolymerization locked their orientations in the solid particles. During UV photopolymerization, a magnetic field was applied to align the anisotropic bipolar $RM257/5CB_{PVA}$ droplets. When the direction of the UV beam was parallel to the axis of the two defect poles of the bipolar $RM257/5CB_{PVA}$ droplets, highly anisotropic LC particles were produced. In the absence of a magnetic field during UV photopolymerization, the resultant LC particles, after the removal of 5CB, had helical

structures owing to the replacement of energetically expensive splay deformation with twisted ones at the defect poles. The detailed internal orientation in the anisotropic LC particles was studied using more than 240 two-dimensional micro-beam X-ray diffraction patterns per particle, which provided the detailed orientation director field in the particle. The porous structure produced by the LC porogen induced the infiltration of 5CB into the LC particles in an LC cell, which caused the rotation of the anisotropic LC particles along the rubbing direction in the polyimide-coated LC cell. The combination of the porous structure and alignment of the LC chains in the anisotropic LC particles exhibited this unique rotating ability in the LC cell.

Keywords: Liquid crystal, microfluidics, anisotropic particle, phase separation, Janus particle.

Introduction: Optically anisotropic birefringent particles are attracting interest for use as potential optical switches[1] and scattering polarizers[2] and might be useful for microfluidic applications such as stirrers and valves.[3] Different types of birefringent particles such as fluoropolymer latex, inorganic (e.g., calcium carbonate vaterite), and liquid crystal (LC) particles are available.[4] Among them, monodisperse birefringent LC particles have been produced from an LC emulsion whose orientational texture could be frozen by photopolymerization.[5] Juodkazis and coworkers have rotated a bulk LC droplet suspended in heavy water using an optical tweezer method.[6] They were able to trap the LC droplet using an optical radiation gradient, and then rotate the LC droplet using radiation forces of circularly polarized light.

The separated LC particles have been prepared using a mini emulsion process, which transforms the prepared polymer into spherical objects.[7] Different side-chain[7] and main-

chain[8] LC polymers were used but in this case, the sizes of the colloids were only in the range of 50–300 nm, which was too small for direct observation using a polarizing optical microscope (POM). Recently, droplet-based microfluidics, which involves the generation of discrete liquid droplets inside microchannels, has witnessed a tremendous growth owing to several advantages such as easy sample handling, reagent mixing, separation, and detection. This technique is sufficiently general for application to a wide range of materials and allows for the production of mono-disperse droplets[9] with controllable sizes ranging from some tens to hundreds of micrometers. We recently reported the preparation of functionalized LC droplets, in which steady-state droplet break-off in the microfluidics channel was used to create monodisperse5-cyanobiphenyl (5CB, a nematic LC at room temperature) droplets in water.[10-13] A droplet was formed at the channel junction. Its size was controlled by the competition between viscous drag and surface tension. Viscous drag tends to pull the drop away from the capillary, and surface tension opposes this pull. When the drop reached a critical size, the viscous drag exceeded the surface tension and break-off occurred.

Stabilizers of surfactants (such as sodium dodecyl sulfate (SDS) and poly(vinylalcohol) (PVA) or amphiphilic polymers can be dissolved in the continuous aqueous phase to stabilize the droplets against coalescence. Apart from preventing coalescence, the stabilizer has an important role in determining the resulting LC configuration within the droplets because it determines the molecular anchoring of the LC molecules onto the surface, analogous to the LCs at the planar surfaces used in display applications. SDS yields homeotropic alignment of the liquid crystal at the surface, thereby resulting in radial droplets having a point hedgehog disclination at the droplet center, while PVA imposes tangential anchoring at the surface resulting in a bipolar configuration with two point defects, referred to as boojum. In contrast to the radial droplet, the bipolar droplet can

be reoriented parallel to the applied electric field for materials with a positive dielectric anisotropy.[14] These orientation director fields of a confined spherical LC droplet are well documented in the literature, and can be confirmed using POM.[14] The configurations in the droplets can be captured through the photopolymerization of reactive LCs. Cairns et al.[15] were able to produce responsive spheres by dispersing reactive 1,4-bis-[4-(6-acryloyloxyhexyloxy)benzoyloxy]-2-methylbenzene (RM257) in glycerol and then the solution was exposed to ultraviolet (UV) light at high temperature in the nematic state of RM257. Glycerol induced the bipolar configuration while curing in the nematic state captured the bipolar director field, which allowed the rotation of the spheres upon the application of an electric field. RM257 is an excellent photopolymerizable diacrylate resin used in a variety of applications with the nematic phase over a wide temperature range; the phase sequence of RM257 is crystal to nematic LC at 87°C and nematic LC to isotropic state at 118°C. However, it is necessary to heat above 87 °C to make it flow in the nematic state.

In this paper, we report on the preparation of various anisotropic particles by using RM257/5CB mixtures, which were found to be completely miscible in the nematic state for high contents of 5CB. They had the ability to flow at room temperature and could be transformed into LC droplets in the microfluidic channel. These mixture droplets could be solidified through UV curing after non-reactive 5CB was extracted. The nematic state of 5CB at room temperature could induce the orientation of RM257 in the mixture droplet owing to their inter-miscibility. This created unique oriented structures in the solid particles after UV curing and 5CB extraction. We found that these mixture droplets, prior to UV curing, exhibited the radial and bipolar configurations of 5CB droplets when coated with SDS and PVA stabilizers, respectively. On the other hand, the resultant solid LC particles, after UV curing, comprised highly porous anisotropic particles and followed the configurations of the

5CB precursor droplets, prior to UV curing. The reorientation of these anisotropic particles having different oriental configurations in the LC cell was investigated. This study might lead to a new strategy for controlling the structures of the anisotropic particles using microfluidics and directional UV photopolymerization in the presence of a magnetic field.

Experimental

Materials: RM257 (Synthron, Germany, **Figure SI 1a**), 5CB (Sigma Aldrich, USA, **Figure SI 1b**), SDS (Duksan, Korea), PVA (Number average molecular weight = 66,000 g/mole, Yakuri, Japan), dichloromethane (DCM, Duksan, Korea), 1-hydroxycyclohexyl phenyl ketone (Sigma Aldrich, USA, **Figure SI 1c**), poly(dimethylsiloxane) (PDMS) kit (Sylgard 184, Dow corning, USA, containing the prepolymer and a cross-linker), (3-aminopropyl)triethoxysilane (APTES, TCI, Japan), and photoresist SU-8 50 (Microchem, USA) were used as-received. Transparent mixtures of RM257/5CB were prepared in DCM at predetermined mixing ratios by means of magnetic stirring. The amount of RM257 in the mixture is denoted as ϕ wt%. These mixtures were heated at 30 °C for 24 h in a vacuum oven to completely remove DCM. Then, 1-hydroxycyclohexyl phenyl ketone (initiator, 2 wt% against RM257/5CB) was added to the solution mixtures with magnetic stirring. Milli-Q water (resistivity higher than 18.2 MΩ cm) was used in all the experiments. Micro slide glass (S9213, Matsunami, Japan, 76×52×1.3 mm^3) was cleaned (Branson5800, USA) using ethanol by employing an ultrasonicator for 5 min, followed by washing with water and drying under nitrogen flow.

Instruments: Differential scanning calorimetry (DSC) of the mixtures was performed on Setaram DSC (131–evo, France). The sample was sealed in an aluminum pan and heated in a

nitrogen atmosphere over the temperature range of 20–140 °C at a heating rate of 10 °C/min.

Microfluidics: The microfluidic flow-focusing devices were fabricated with PDMS elastomer using conventional photolithography involving SU-8 50 photoresist on a silicon wafer. PDMS was prepared by thoroughly mixing the pre-polymer and cross linker in the recommended ratio of 10:1 (w/w), and degassing for 40 min in a desiccator to remove any remaining air bubbles. The final mixture was poured into a silicon wafer mold and cured inside an oven at 65 °C for 4 h before removing it from the structured silicon wafer. The patterned PDMS and pre-cleaned micro slide glass was immersed in an APTES (2 wt%) ethanol solution for improving the hydrophilicity in the channel while the unreacted APTES was removed by sonication in water for 1 min.[16] The patterned piece of PDMS was bonded to the micro slide glass using short oxygen plasma treatment (46 s, Femto Science Inc., Korea). **Figure SI 2a** shows the schematic of the microchip and dimensions of the microfluidics channel used in this study and **Figure SI 2b** is its photographic image. The widths of the inlet channels, orifice, and outlet channel were 40, 40, and 160 μm, respectively, while the channel depth was 80 μm. The microchannels were immediately filled with water to maintain hydrophilicity in the channel until the chip was used.

Fabrication of anisotropic particles: The microfluidic chip was mounted under an inverted biological microscope (NSI-100, Samwon, South Korea). The liquid samples were supplied to the microfluidic device *via* flexible plastic tubing (Norton, USA, I.D. 0.51 mm, O.D. 1.52 mm) attached to precision syringes (SGE Analytical Science, Australia) operated by digitally-controlled syringe pumps (KDS 100 series, KD Scientific, USA). The flows of the fluids to the microfluidic channels were controlled using two independent syringe pumps. The

formation of on-chip droplets was photographed using an STC-TC83USB-AS camera (Sen Tech, Japan) attached to the inverted microscope. The images of the droplets were observed under the POM (ANA-006, Leitz, Germany) in the cross-polar state. The dispersed phase consisting of a RM257/5CB mixture was slowly injected into the middle inlet, and the continuous phase containing either SDS or PVA (2 wt%) was injected into the other inlets in a direction perpendicular to the dispersed phase (**Figure SI 2**). Both the phases met at the junction and the formation of droplets took place when the fluids were crossing the neck of the channel. Typical flow rates used for the formation of droplets were 0.03 and 0.3 mLh^{-1} for the dispersed and continuous phases, respectively, unless otherwise mentioned. The RM257/5CB droplets coated with either SDS or PVA were extracted from the microchip and collected in a storage reservoir, which was made by gluing a thin silicon rubber sheet onto the glass slide.

UV curing of anisotropic particles under a magnetic field: Two configurations of the horizontal and vertical magnet set-ups were used to align the RM257/5CB droplets as shown in **Figure SI 3**. The horizontal configuration (**Figure SI 3a**) used bar magnets and the direction connecting N and S magnetic poles was perpendicular to the UV beam direction. The vertical configuration (**Figure SI 3b**) used hole magnets and the direction connecting N and S magnetic poles was parallel to the UV beam direction. The space between the two bar magnets was 4 cm while the diameter of the hole magnet was 3 cm. The RM257/5CB droplets in the slide glass container were polymerized using a UV lamp (SPOT UV/Inno-cures 100 N, 365 nm, 100 W, 2000 mW cm^{-2}) positioned above the sample container for directional UV photopolymerization with and without magnets. The UV beam was focused using a focusing lens (adjustable collimating adaptor, Lumen dynamics) on the sample and

reflected from the mirror under the sample container for homogenous UV curing. Unless specified otherwise, the distance between the container and light was 7 cm and the polymerization time was 360 s. After UV curing of the RM257/5CB droplets, 5CB was extracted several times from the droplet with ethanol. RM257/5CB droplets were put into the vial containing 20 mL ethanol for 24 h and then ethanol was replaced with fresh one two times. The poly(RM257) LC particles after 5CB extraction were dried in a vacuum oven for one day.

Observation of anisotropic particles: These slide glass containers were then placed under POM (Leitz, ANA-006 Germany) in a cross polar state. The droplets in the container were observed before and after UV curing and 5CB extraction. The UV-cured LC particles were redispersed in 5CB (10 wt%) and injected into a cell, which was made up of two polyimide (PI)-rubbed glass slides sandwiching 90 μm-thick Mylar spacers at the edges with parallel rubbing directions of two glasses. The motion of the anisotropic LC particles in the cell was recorded under POM using a STC-TC83USB-AS camera (Sen Tech, Japan).

Orientation of anisotropic particles: Wide angle X-ray diffraction (WAXS) measurements were carried out in the synchrotron beam line P03 at DESY, Germany with a micro-focus beam size of 0.9 × 0.9 μm^2. The wavelength of radiation (λ) was 0.8266 Å and the sample to detector distance was 181.4 mm. The scattering patterns were collected by a High-resolution CCD (photonic science, UK) with 1475×1475 pixels (pixel size: 122.4 × 122.4 μm2). The samples were translated through the microbeam stepwise, and the WAXS patterns were recorded at each step with the exposure time of 10 s. I (s) = I (s_1,s_2) in the patterns covers the region 0.006 $nm^{-1} \leq |s_1,s_2| \leq 0.42\ nm^{-1}$, where s = ($s_1$,$s_2$) is the scattering vector along the two

axes perpendicular to the beam with its modulus defined by $|s| = s = (2/\lambda) \sin \theta$, where 2θ is the scattering angle. In real space, the monitored area entirely covers the LC particles. The scattering patterns were subtracted from the pattern without a sample. The radiation damage was checked using WAXS patterns taken from the same spot repeatedly. No radiation damage was detected up to an exposure time of 3 min.

Results and discussion

Phases of RM257/5CB mixtures: **Figure SI 1** shows the chemical structures of RM257, 5CB, and an initiator of 1-hydroxycyclohexyl phenyl ketone. The phase behavior of the RM257/5CB mixtures was examined to identify suitable mixtures for the preparation of the LC droplets. **Figure SI 4a** shows the DSC thermograms of the RM257/5CB mixtures at ϕ = 0 to 100 wt%, prior to photopolymerization. Two endothermic peaks at ϕ = 100 wt% (pure RM257) were observed at 70 and 128 °C, owing to the crystalline to nematic (T_{kn}), and nematic to isotropic (T_{ni}) transitions, respectively. The T_{ni} peaks shifted continuously to lower temperatures with the increasing ϕ. **Figure SI 4b** shows these transition temperatures as a function of ϕ. The T_{kn} transition was observed only at ϕ = 100 to 60 wt%, even though the T_{ni} transitions were observed at all mixing ratios. An increase in T_{ni} with increasing ϕ was consistent with the results reported by Stapert et al. using RM257/E7 mixtures.[17] E7 is a liquid crystal mixture consisting of several cyanobiphenyls with long aliphatic tails used commercially in liquid crystal displays. A decrease in T_{kn} with decreasing ϕ was attributed to the melting temperature depression of RM257 by mixed 5CB, which was normally observed for binary crystalline/amorphous mixtures. Therefore, the mixtures at ϕ = 10–50 wt% showed a single nematic phase while those at ϕ = 60–90 wt% exhibited crystalline + nematic phases at room temperature. The solutions at ϕ = 0–50 wt% between the two slide glasses were

observed with POM in the cross-polar state, as shown in **Figure SI 4c**. The POM images at ϕ = 10–50 wt% at room temperature revealed typical nematic marble textures, thereby suggesting that the mixtures represented a completely miscible nematic phase at these mixing ratios. The nematic marble texture is normally observed in thin samples, particularly for substrates, which have not been rubbed or treated in any way.[18] The RM257/5CB mixtures at $\phi \geq 20$ wt% were too viscous to flow in the channel; as a result, the mixtures at ϕ = 5–15 wt% were used for further experiments.

RM257/5CB droplet: **Figure 1** shows the optical microscopy images of the droplets of the RM257/5CB mixture (ϕ = 15 wt%) as a function of the flow rate of the continuous aqueous phase, Q_c, for a fixed flow rate of the disperse phase, Q_d of 0.03 $mLh^{-1}$with 2 wt% SDS in the continuous phase. Over the entire range of Q_cs, the droplets were successfully produced at the flow-focusing region in the microfluidic channel. The sizes of the droplets at Q_c= 0.1, 0.2, 0.3, and 0.5 mLh^{-1}were 74, 65, 62, and 57 μm, respectively, with low polydispersity (not exceeding 1%). Similar results were obtained for other RM257/5CB mixtures. The droplets produced at Q_c = 0.3 mLh^{-1} and Q_d = 0.03 mLh^{-1}were used in further experiments in this work unless otherwise mentioned.

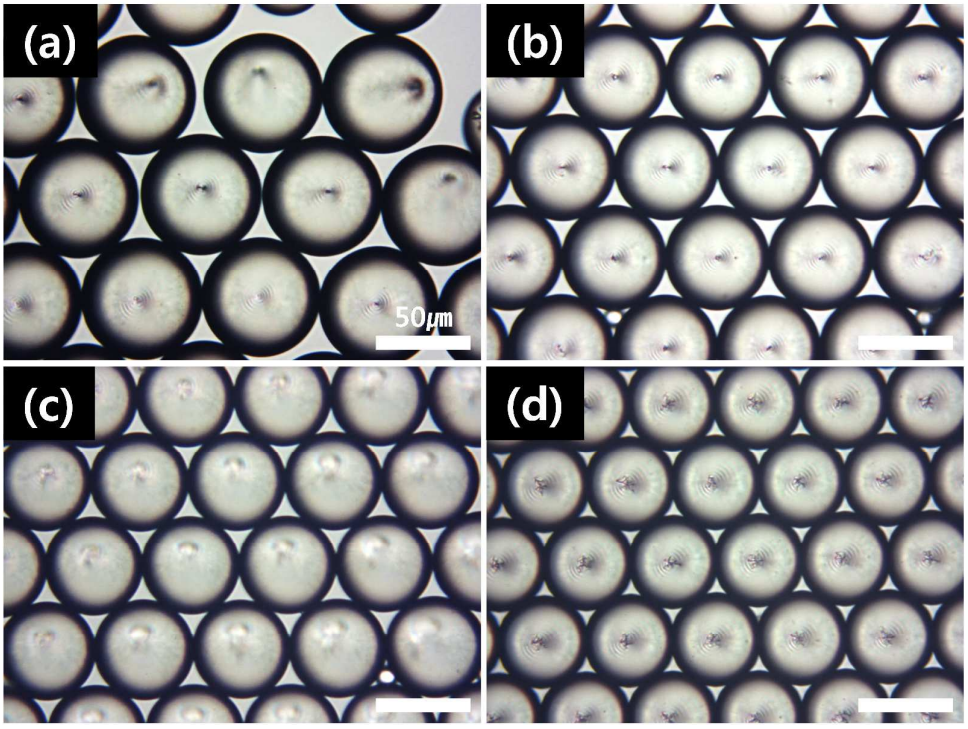

Figure 1. Optical microscopy images of droplets of RM257/5CB mixture (ϕ = 15 wt%) at Q_c = (a) 0.1, (b) 0.2, (c) 0.3, and (d) 0.5mLh^{-1} for a fixed Q_d of 0.03mLh^{-1} with 2 wt% SDS in continuous phase.

Figure 2 shows the POM images of the RM257/5CB droplets at ϕ = 0, 5, 10 and 15 wt% with SDS (or PVA) in the continuous phase under crossed polarizers. Without SDS and PVA in the continuous phase, the RM257/5CB droplets were frequently plugged and the stable droplets could not be produced. The RM257/5CB droplets with SDS (RM257/5CB$_{SDS}$) and PVA (RM257/5CB$_{PVA}$) showed the radial and bipolar configurations, respectively, for all the mixing ratios tested herein. A pure 5CB droplet with SDS and PVA coating was known to have radial and bipolar configurations, respectively. As a result, the RM257/5CB droplet followed the configuration of the pure 5CB droplet owing to the complete miscibility between RM257 and 5CB. The radial configuration having a point hedgehog disclination at

the drop center could be attributed to the horizontal penetration of the alkyl chains of SDS into the LC droplet against the surface of the LC droplet. This made the 5CB monomers orient perpendicularly to the surface of the 5CB droplet. The bipolar configuration, referred to as boojum, was because of the tangential anchoring of 5CB with two point defects at the poles. These director-field configurations are well documented in the literature[5] and could be confirmed using POM. The insets of **Figure 2** show the schematic representations of the director field of the RM257/5CB droplets with radial and bipolar configurations.

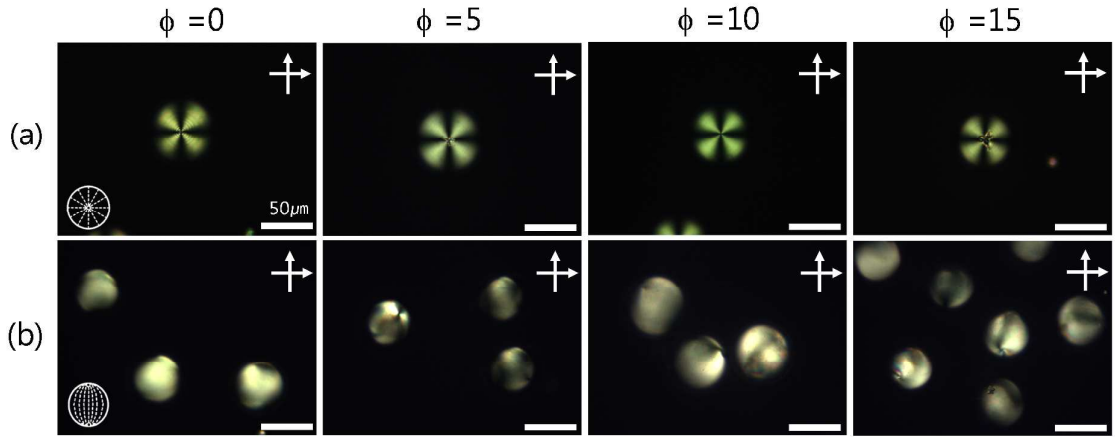

Figure 2. POM images of the RM257/5CB droplets at ϕ = 0, 5, 10, and 15 wt% with 2 wt% (a) SDS or (b) PVA in continuous phase under crossed polarizers before UV curing; insets are schematic representations of director field of 5CB droplets with radial and bipolar configurations while arrows represent directions of crossed polarizers.

Alignment of RM257/5CB droplet using a magnetic field: The anisotropic bipolar LC droplets can be aligned using an external magnetic (or electric) field. Depending on the sign of the dielectric constant of the material, the bipolar LC droplet can align in either parallel or perpendicular direction to the field. Since the major component of 5CB in the RM257/5CB mixture has a + Δε symmetry, the axis connecting two defect poles in the bipolar droplets

tended to align parallel to the direction of the magnetic field. In the movies and final POM images under crossed polarizers during the application of the magnetic field to the RM257/5CB$_{SDS}$ (ϕ = 15 wt%) droplets with the horizontal (movie SI 1, **Figure 3a**) and vertical (movie SI 2, **Figure 3b**) magnet set-ups, no movement of the RM257/5CB$_{SDS}$ droplets was observed. This was because the centro-symmetric radial RM257/5CB$_{SDS}$ droplets could not be oriented by an external magnetic field. However, in the movies and final POM images under crossed polarizers during the application of the magnetic field to the RM257/5CB$_{PVA}$ droplets with horizontal (RM257/5CB$_{PVA,horizontal}$, movie SI 3, **Figure 3c**) and vertical (RM257/5CB$_{PVA,vertical}$, movies SI 4, **Figure 3d**) magnet set-ups, it was observed that the RM257/5CB$_{PVA}$ droplets were slowly aligned in the direction connecting the two defect poles along the magnetic field direction. As a result, the two defect poles were parallel to the surface of the reservoir for the RM257/5CB$_{PVA,horizontal}$ (**Figure 3c**) but only one pole defect was visible for the RM257/5CB$_{PVA,vertical}$ (**Figure 3d**) owing to the vertical alignment of the two defect poles. This alignment of the RM257/5CB$_{PVA}$ droplets was because of the anisotropic nature of the bipolar droplet. The ability of the rotation strongly suggested that the magnitude of the dipole moment of the RM257/5CB$_{PVA}$ droplet was strong enough for the RM257/5CB$_{PVA}$ droplets to be aligned along the direction of the magnetic field.

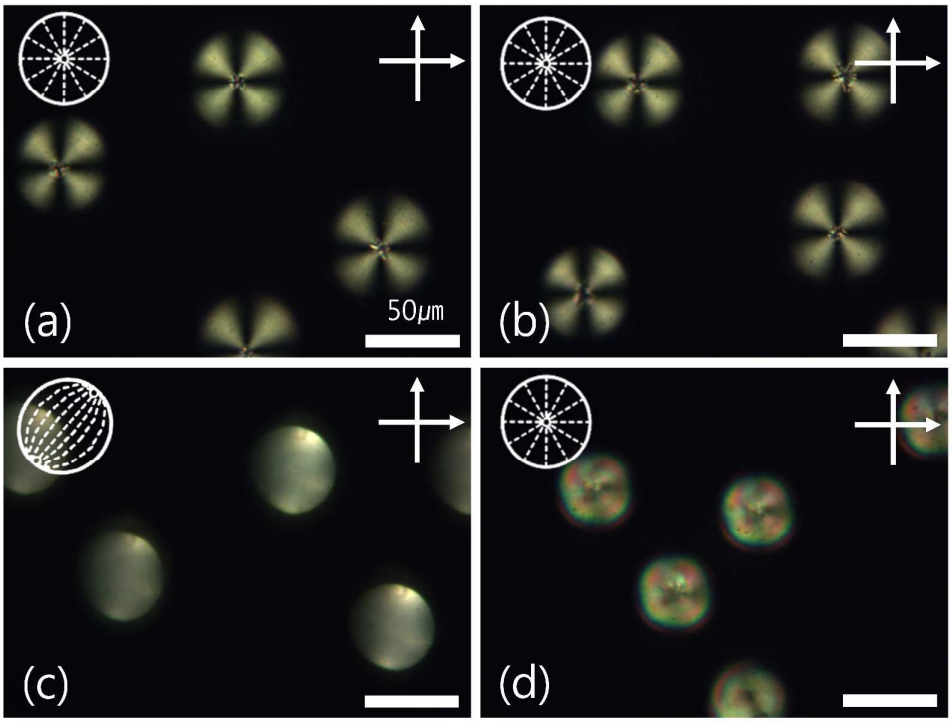

Figure 3. POM images of (a, b) RM257/5CB$_{SDS}$ and (c, d) RM257/5CB$_{PVA}$ droplets (ϕs for both are 15 wt%) aligned by magnetic field with (a, c) horizontal and (b, d) vertical magnet arrangements.

Movie SI 1. Movies during reorientation of (a, b) RM257/5CB$_{SDS}$ and (c, d) RM257/5CB$_{PVA}$ droplets (ϕs for both are 15 wt%) aligned by a magnetic field with (a, c) horizontal and (b, d) vertical magnet arrangements.

UV photopolymerization of RM257/5CB droplet: Post photo-polymerization of the RM257/5CB droplets was performed off-chip using a focused UV beam under the horizontal or vertical magnet set-up. The cross-linked structure of the LC particle could be studied in ethanol (one of the good solvents for poly(RM257)), which would swell the LC particle. No disintegration of the LC particle in ethanol was observed, thereby indicating that the

polymerization of RM257 in 5CB was successful. The internal orientation of the swelled LC particles in ethanol could be observed using POM. However, it was relatively difficult to see the orientation of the dried LC particles because they shrank and winkled owing to the pores (dried particle will be discussed in a later section). **Figure 4a** shows the POM image of the LC particle made from RM257/5CB$_{SDS}$ droplets (LC$_{SDS}$ particle) in ethanol. The image shows a spherical shape with a Maltese cross under the crossed polarizers. The rotation of the LC$_{SDS}$ particle by 45° made the Maltese cross to rotate by the same degree simultaneously. This result indicated that the orientation of the LC$_{SDS}$ particle followed the radial orientation of the RM257/5CB$_{SDS}$ droplet (before UV curing) while the chain orientation of poly(RM257) in the droplet was locked by UV photopolymerization. **Figure 4b** shows the POM image of the LC particle made from the RM257/5CB$_{PVA}$ droplet without the magnets (LC$_{PVA,\ random}$ particle) during UV irradiation. The LC$_{PVA,\ random}$ particle was positioned with the line connecting their two defect poles along the polarizer's direction. A black line starting at the defect poles was observed at a certain angle against the polarizer's direction. This POM image was a typical twisted structure.[19] The GI measurement against the φ showed the lowest value at φ_{min}=100° for the LC$_{PVA,\ random}$ particle as shown in **Figure 5**. This ϕ_{min} was known to be dependent on the pitch direction of the chirality. The φ_{min}=100° is one of the examples while other φ_{min} values around 90° were found in other LC$_{PVA,\ random}$ particles. The deviation of φ_{min} from 90° indicated that the initial bipolar orientation of the RM257/5CB$_{PVA}$ droplet (which should be 90°) changed to the twisted structure during UV photopolymerization. Tortora et al. explained that the twisted structure in the bipolar particle was due to chirality induction as a replacement of energetically expensive splay packing in the curved bipolar tactoidal shape with twisted packing.[20-21] As shown by Williams et al.[22] and experimentally verified using an earlier report,[23] such a structure was energetically

preferable if the elastic constant K_{22} of twist was sufficiently small as compared to the splay K_{11} and bend K_{33} constants, thereby satisfying the following condition of $K_{22}/K_{11} \leq 2.32(1 - K_{33}/K_{11})$. A bipolar structure shows splay deformation near the defect poles and bend deformation near the equatorial plane. As noted by Prinsen and van der Schoot,[24] the Williams condition was much harder to fulfill for the bipolar droplet because the solid angle, wherein the director was splayed near the defect pole was small. The twisted structure observed in the $LC_{PVA,\ random}$ particle might have resulted from a small fraction of the polymerizable RM257 content in the mixture (e.g., ϕ = 15 wt%), and thus, a large room existed for twisting poly(RM257) chains at the poles leading to low K_{22}. This result demonstrated a simple pathway for the macroscopic chirality induction in an organic system with no molecular chirality, as the only requirements were tangential orientation and curved shape of confinement.

Figures 4c and **d** show the POM images of the $LC_{PVA,\ horizontal}$ and $LC_{PVA,\ vertical}$ particles in ethanol, respectively. The $LC_{PVA,\ horizontal}$ and $LC_{PVA,\ vertical}$ particles were positioned with the line connecting their two defects parallel to the polarizer's direction. The center of the particle was blacker compared to the other parts, and the defect poles were black. The black color implied a parallel orientation with the polarizer. This POM image was owing to the bipolar orientation of the $LC_{PVA,\ particle}$ wherein the directors at the center and the two poles were parallel to one of the crossed polarizers. When the crossed polarizers were oriented by 45°, the black color changed to green, and the poles became bright. This was because the birefringence of the oriented material in the POM image under crossed polarizers was highest when the director of the oriented material was along the 45° direction from the polarizer. **Figure 5** shows the GI values of the $LC_{PVA,\ horizontal}$ and $LC_{PVA,\ vertical}$ particles as a function of φ. The lowest values were found at φ_{min} = 90° for both $LC_{PVA,\ horizontal}$ and $LC_{PVA,\ vertical}$

particles indicating that the overall orientation direction of the $LC_{PVA,\ horizontal}$ and $LC_{PVA,\ vertical}$ particles was along the line connecting two defect poles without twisting. The difference between the $LC_{PVA,\ random}$ and $LC_{PVA,horizontal/vertical}$ particles was the application of the magnetic field during photopolymerization. The magnetic field might hold the RM257/5CB droplets during UV photopolymerization such that it could polymerize the RM257 monomer without twisting. This result also indicated that the UV beam momentum could rotate the LC droplet in the energetically preferable direction during polymerization to get a twist configuration when no confinement by external force (such as magnetic field) was applied. Thus, the twisted structure might be observed only for the $LC_{PVA,\ random}$ droplets.

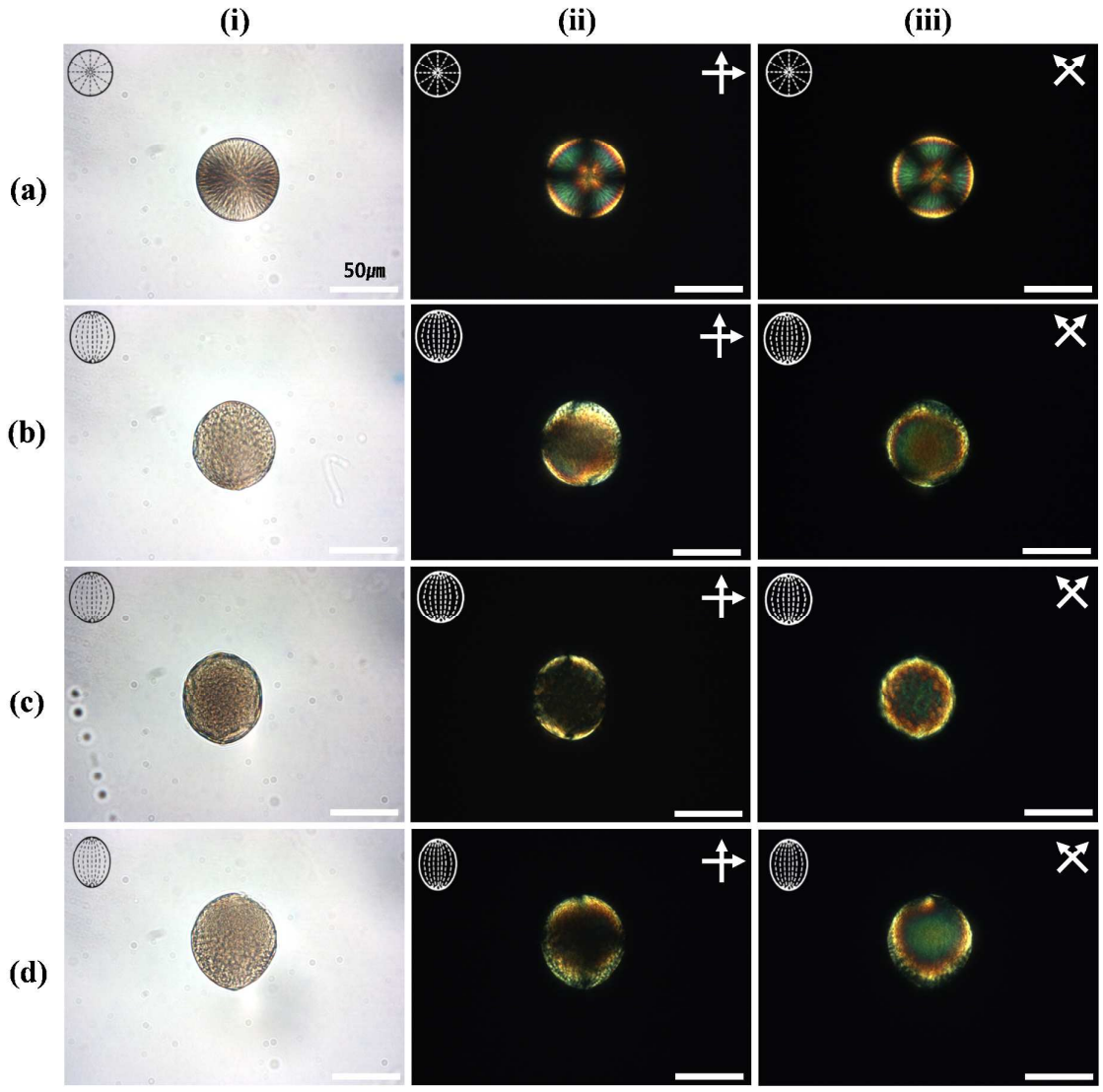

Figure 4. Optical microscopy images of (a) LC_{SDS}; (b) $LC_{PVA,\ random}$; (c) $LC_{PVA,\ horizontal}$; and (d) $LC_{PVA,\ vertical}$ particles in ethanol (i) without and (ii, iii) with crossed polarizers; directions of crossed polarizers are along (ii) direction connecting defect poles of LC_{PVA} particle; and (iii) 45° rotation from (ii) direction, as shown by arrows.

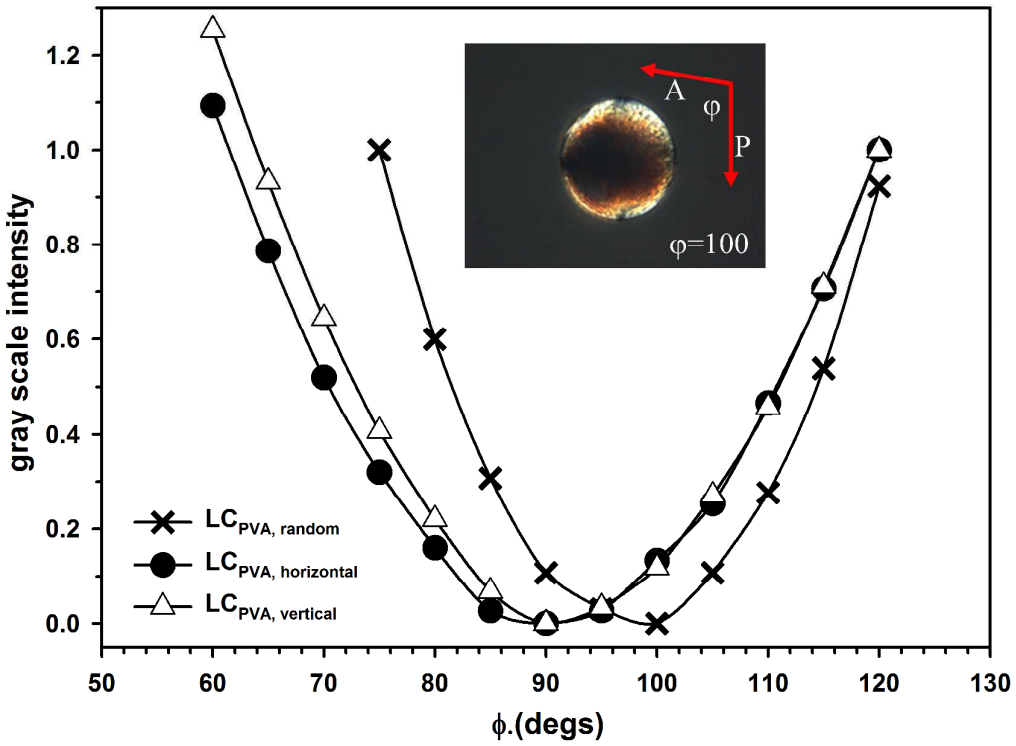

Figure 5. GI of POM images of (×) $LC_{PVA,\ random}$, (•) $LC_{PVA,\ horizontal}$, and (Δ) $LC_{PVA,\ vertical}$ particles as a function of φ; φ is angle between a polarizer (P) and an analyzer (A) with the direction connecting two defect poles parallel to P as shown in inset.

Structures of anisotropic LC particles: As the droplets of the RM257/5CB mixtures were irradiated by UV light, a photoreaction to form the cross-linked poly(RM257) solid structure occurred with simultaneous phase separation, which induced the diffusion of RM257 monomers and 5CB into polymer-rich and polymer-poor (5CB-rich) regions, respectively. **Figure 6** shows the SEM images of the dried LC particles. The UV-exposed hemispheres of all the examined LC_{SDS} and LC_{PVA} particles showed smoother and more wrinkled surfaces compared to the unexposed hemispheres. The UV-exposed hemisphere would have had a faster polymerization rate compared to that in the unexposed hemisphere. As a result, this

difference in the polymerization rate created a difference in the morphology of each hemisphere. While slow polymerization could provide adequate time for phase separation to yield the conceivable 5CB-rich domains, fast polymerization could not do so to yield large domains. The small phase-separated domain in the UV-exposed hemisphere yielded a large interfacial area wherein less cross-linking occurred. The less cross-linked hemisphere swelled more than the other. Thus, the UV-exposed hemisphere yielded the swelled compact structure while the other had the more porous open structure. This result indicated that the directional UV photopolymerization could induce the Janus-like LC particles owing to the relative difference in the rate between polymerization and phase separation. The dried LC_{SDS} particles (**Figure 6a**) were close to a spherical shape with wrinkled surface observed on the UV-exposed hemisphere. However, the dried $LC_{PVA,\ vertical}$ (**Figure 6b**) an`d $LC_{PVA,\ horizontal}$ particles (**Figure 6c**) were anisotropic prolate spheroids with a long axis connecting two defect poles. The overall shape looked like a rice seed. Fernandwz-Nieves et al. reported bipolar colloids of anisotropic geometry, which had been obtained by stretching the polymerizable LC emulsion embedded in a PVA thin film prior to photopolymerization.[25] However, these anisotropic particles produced herein were unique compared to the mechanically deformed anisotropic particles because the spontaneous anisotropic particles were produced during UV photopolymerization. The $LC_{PVA,\ random}$ particles showed the twisted structure as shown in the groove on the surface of the UV-exposed hemisphere (**Figure 6d**). This structure was consistent with the swelled structure in ethanol as discussed in the previous section (**Figure 4b**). The degree of the anisotropy could be measured by the ratio between the diameters of the long and short axes of a prolate spheroid. The degree of the anisotropy for $RM257/5CB_{PVA,\ horizontal}$ and $RM257/5CB_{PVA,\ vertical}$ were 1.9 and 2.1, respectively, thereby indicating that more anisotropic particles could be produced using a

vertical magnet set-up due to the same UV beam direction with the average director orientation direction

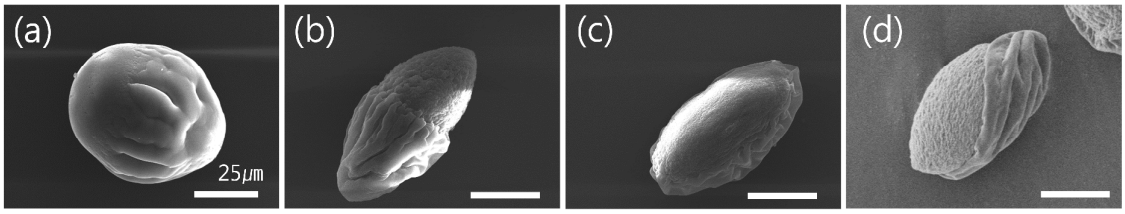

Figure 6. SEM images of dried (a) LC_{SDS};(b)$LC_{PVA,\ vertical}$;(c)$LC_{PVA,\ horizontal}$; and (d) $LC_{PVA,\ random}$particles.

The internal orientation was studied at the micro-beam line P03 at DESY. **Figure 7** shows the selective two-dimensional X-ray diffraction patterns of the LC_{SDS} and $LC_{PVA,\ vertical}$ particles with orientation vector fields at the individual positions inside the particle. The strong peak at s =0.222Å^{-1} (d = 4.5 Å) represented the mean distance between the mesogenic groups in the nematic state. The lateral packing of the mesogenic groups was perpendicular to the chain axis of poly(RM257). Thus, the direction of this peak represented the direction perpendicular to the chain direction. The distribution of the chain orientation in the particle could be represented by the orientation vector field of the chain direction, which could be measured from the azimuthal maximum position of the individual patterns at s = 0.222Å^{-1}(d = 4.5 Å). The orientation vector field of the $LC_{PVA,vertical}$ particle (**Figure 7a**) was along the parabolic line connecting the two defect poles and that of the $LC_{SDS,}$ particle (**Figure 7b**) was from the center of the particle, thereby indicating that the orientation of the LC_{PVA} and $LC_{SDS,}$particles followed the orientation of their precursors of bipolar $RM257/5CB_{PVA}$ and radial $RM257/5CB_{SDS}$ droplets, respectively. This result demonstrated the internal orientation of the anisotropic LC particle induced by the surface anchoring, for the first time, using micro

X-ray beam. The average full width at half maximum was approximately ~ 40°, which was not much different from the values seen at the other positions.

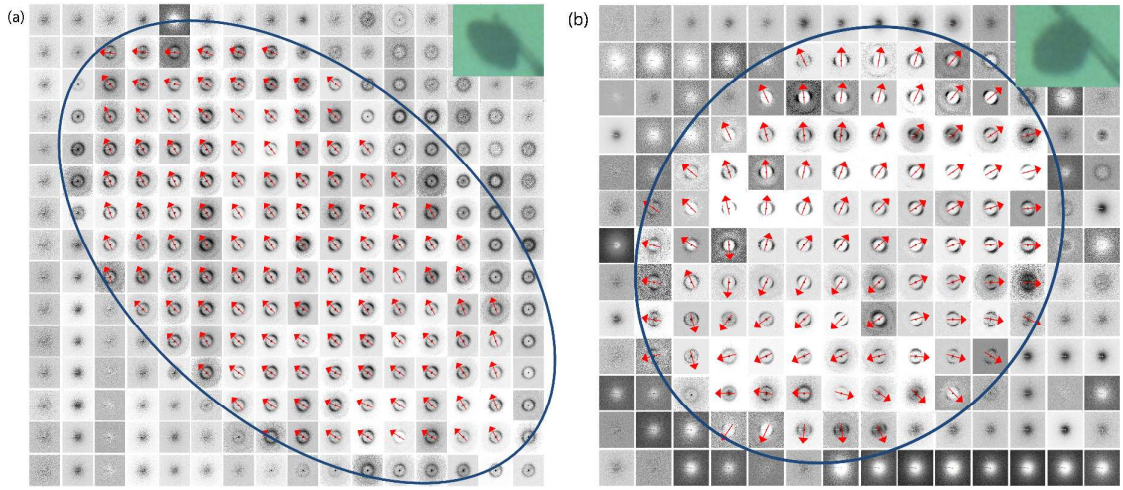

Figure 7. Two-dimensional X-ray diffraction patterns with the orientation vector field at individual positions inside: (a) $LC_{PVA,\ vertical}$; and (b) LC_{SDS} particles; Insets in (a) and (b) are the photographs of $LC_{PVA,\ vertical}$ and LC_{SDS} particles on the glass needle during X-ray measurements, respectively.

Alignment of anisotropic LC particles in LC cell: The anisotropic LC_{PVA} particles have pores with a certain chain orientation, which could be controlled by anchoring conditions at the surface and an external magnetic field during photopolymerization. 5CB in the LC cell could be infiltrated into the porous anisotropic LC_{PVA} particles. The infiltrated 5CB could be anchored using the poly(RM257) in the LC_{PVA} particle and following the orientation along the interface of the pore. The orientation of the infiltrated 5CB might be different from the global 5CB orientation in the LC cell. This difference could create the elastic force required for rotating the LC particles along the global orientation in the LC cell. The alignments of the $LC_{PVA,horizontal,}$ and $LC_{PVA,\ vertical}$ particles, which have different internal orientations and pore

structures, were tested in the LC cell with more than 50 particles. **Figure SI 5** shows the POM images of the selective anisotropic LC_{PVA} particles in the LC cell under crossed polarizers, which were rotated 45° against the horizontal global orientation of the cell for better visualization by the bright background of the LC cell. **Figure 8** shows the distribution of the aligned orientation of the anisotropic LC_{PVA} particles in the LC cell, which was measured by counting the number of LC_{PVA} particles oriented at a certain angle, χ, defined as the angle between the director of the LC cell and long axis of the particle. Nearly all $LC_{PVA,\ vertical}$ particles were oriented along the director of the LC cell (χ = 0°) indicating that the LC particles were aligned along the director of the LC cell by the LC elastic force exerted on the particles. Interestingly, $LC_{PVA,\ horizontal}$ particles showed a wide range of distribution with regard to the orientation in the LC cell probably owing to the perpendicularity of the UV direction to the director orientation in the droplet. This might have resulted in an unaligned pore structure. Thus, the highly alignable LC particles in the LC cell could be produced when the UV beam and orientation of the polymerizable monomers were parallel to each other during photopolymerization.

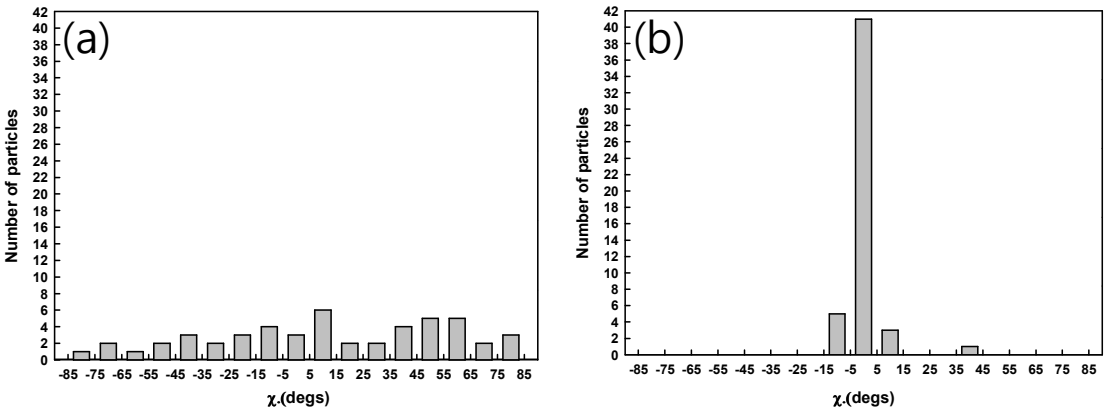

Figure 8. Distribution of the aligned orientation of anisotropic (a) $LC_{PVA,\ horizontal}$; and (b) $LC_{PVA,\ vertical}$ particles in an LC cell against the angle, χ, which is defined as the angle between

the director of the LC cell and the long axis of the particle.

Conclusions: The highly anisotropic porous LC_{PVA} particles were fabricated by microfluidics and directional UV photopolymerization by using RM257/5CB mixtures and PVA coating on the droplet surface and compared to the LC_{SDS} particles which were produced with the same method except SDS coating. The directional UV photopolymerization of the precursor $RM257/5CB_{PVA}$ droplet using magnetic field directing along the average director of the $RM257/5CB_{PVA}$ droplet fixed the internal orientation of its bipolar configuration leading to a highly anisotropic prolate spheroid LC particle although that of the precursor $RM257/5CB_{SDS}$ droplet fixed the radial configuration. The resultant LC particles had different morphologies between the two opposite hemispheres depending on the direction of the UV irradiation, thereby leading to Janus-like particles. The porous LC_{PVA} particles aligned along the direction of the global orientation in the LC cell by the elastic force generated from the different orientation between the anchored 5CB inside the particle and globally oriented 5CB in the LC cell while the LC_{SDS} particles did not due to the isotropic radial chain orientation in the particle.

Acknowledgement: This work was supported by the National Research Foundation of Korea (NRF-2011-0020264) and XFEL project (MEST and PAL).

Reference

[1] D. R. Cairns, M. Sibulkin and G. P. Crawford, *Applied Physics Letters*, 2001, **78**, 2643-2645.

[2] I. Amimori, N. V. Priezjev, R. A. Pelcovits and G. P. Crawford, *Journal of Applied Physics*, 2003, **93**, 3248-3252.

[3] A. Fernandez-Nieves, *Soft Matter* 2006, **2**, 105-108.

[4] K. Sandomirski, S. Martin, G. Maret, H. Stark and T. Gisler, *J. Phys. Condens. Matter*, 2004, **16**, S4137-S4144.

[5] P. S. Drzaic, ed., *Liquid Crystal Dispersion*, World Scientific, Singapore, 1995.

[6] S. Juodkazis, M. Shikata, T. Takahashi, S. Matsuo and H. Misawa, *Applied Physics Letters*, 1999, **74**, 3627-3629.

[7] M. Vennes, R. Zentel, M. Rössle, M. Stepputat and U. Kolb, *Advanced Materials*, 2005, **17**, 2123-2127.

[8] Z. Yang, W. T. S. Huck, S. M. Clarke, A. R. Tajbakhsh and E. M. Terentjev, *Nat Mater*, 2005, **4**, 486-490.

[9] P. B. Umbanhowar, V. Prasad and D. A. Weitz, *Langmuir*, 1999, **16**, 347-351.

[10] W. Khan, J. H. Choi, G. M. Kimb and S. Y. Park, *Lab Chip*, 2011, **11**, 3493-3498.

[11] W. Khan, J.-M. Seo and S. Y. Park, *Soft Matter*, 2011, **7**, 780-787.

[12] J. Kim, J. Joo and S.-Y. Park, *Particle & Particle Systems Characterization*, 2013, **30**, 981-988.

[13] J. Kim, M. Khan and S.-Y. Park, *ACS Appl. Mater. Interfaces*, 2013, **5**, 13135-13139.

[14] R. Ondris-Crawford, E. P. Boyko, B. G. Wagner, J. H. Erdmann, S. Žumer and J. W. Doane, *Journal of Applied Physics*, 1991, **69**, 6380-6386.

[15] D. R. Cairns, M. Sibulkin and G. P. Crawford, *Applied Physics Letters*, 2001, **78**, 2643-2645.

[16] M. J. Lee, N. Y. Lee, J. R. Lim, J. B. Kim, M. Kim, H. K. Baik and Y. S. Kim, *Advanced Materials*, 2006, **18**, 3115-3119.

[17] H. R. Stapert, S. del Valle, E. J. K. Verstegen, B. M. I. van der Zande, J. Lub and S. Stallinga, *Advanced Functional Materials*, 2003, **13**, 732-738.

[18] G. Friedel, *Annales de Physique* 1922, **18**, 273-474.

[19] L. Tortora and O. D. Lavrentovich, *Proceedings of the National Academy of Sciences*, 2011, **108**, 5163-5168.

[20] G. E. Volovik and O. D. Lavrentovich, *Sov. Phys. JETP*, 1983, **58**, 1159-1166.

[21] O. D. Lavrentovich and V. V. Sergan, *Il Nuovo Cimento D*, 1990, **12**, 1219-1222.

[22] R. D. Williams, *J. Phys. A: Math. Gen*. 1986, **19**, 3211-3222.

[23] O. D. Lavrentovich and V. V. Sergan, *Il Nuovo Cimento D*, 1990, **12**, 1219-1222.

[24] P. Prinsen and P. v. d. Schoo, *J. Phys.: Condens. Matter*, 2004, **16**, 8835-8850.

[25] A. Fernández-Nieves, G. Cristobal, V. Garcés-Chávez, G. C. Spalding, K. Dholakia and D. A. Weitz, *Advanced Materials*, 2005, **17**, 680-684.